

Development of a low-background HPGe detector at Kamioka Observatory

K. Ichimura^{1, *}, H. Ikeda¹, Y. Kishimoto^{1,3}, M. Kurasawa¹, A.A. Suzuki¹,
Y. Gando^{1,6}, M. Ikeda^{2,3}, K. Hosokawa², H. Sekiya^{2,3}, H. Ito⁴,
A. Minamino⁵, and S. Suzuki⁵

¹*Research Center for Neutrino Science, Tohoku University, 6-3 Aoba,
Aramaki, Aoba-ku, Sendai, Miyagi 980-8578, Japan*

²*Kamioka Observatory, Institute for Cosmic Ray Research, The University
of Tokyo, 456 Higashi-Mozumi, Kamioka, Hida, Gifu 506-1205, Japan*

³*Kavli Institute for the Physics and Mathematics of the Universe (WPI),
The University of Tokyo Institutes for Advanced Study, The University of
Tokyo, 5-1-5 Kashiwanoha, Kashiwa, Chiba 277-8582, Japan*

⁴*Department of Physics and Astronomy, Faculty of Science and Technology,
Tokyo University of Science, 2641 Yamazaki, Noda, Chiba 278-8510, Japan*

⁵*Department of Physics, Yokohama National University, 79-5 Tokiwadai,
Hodogaya-ku, Yokohama, Kanagawa, 240-8501, Japan*

⁶*Department of Human Science, Obihiro University of Agriculture and
Veterinary Medicine, Inada-cho Nishi 2-11, Obihiro, Hokkaido 080-8555,
Japan*

*E-mail: ichimura@awa.tohoku.ac.jp

.....
A new ultra-low background high-purity germanium (HPGe) detector has been installed at the Kamioka underground experimental site. The background count rate in the energy range from 40 keV to 2700 keV is about 25% lower than that of the first HPGe detector installed in 2016, which has the same detector specification and similar shielding geometry. This paper describes the shielding configuration, including the cleaning of the material surface, the comparison of calibration data and simulation, the time variation of the background spectra, the sample measurement procedure, and some results of the radioactivity in the selected samples.
.....

Subject Index H20

1 Introduction

Material screening with high sensitivity is one of the important tasks for the current and next-generation rare event search experiments. For example, the SK-Gd project [1] requires that the concentration of radioactive impurities in $\text{Gd}_2(\text{SO}_4)_3 \cdot 8\text{H}_2\text{O}$ should be less than 0.5 mBq kg^{-1} of the latter segment of U-chain (^{226}Ra) and 0.05 mBq kg^{-1} of the latter segment of the Th-chain (^{228}Ra) for the precise measurements of the solar neutrino spectrum [2]. The KamLAND-Zen experiment [3], aiming to explore the neutrinoless double beta decay of ^{136}Xe , plans to use a scintillation film and a wavelength shifter to enhance the sensitivity [4]. The radioactivities of the scintillation film and the wavelength shifter are required to be equal to or less than $\mathcal{O}(1 \text{ ppt})$ for ^{238}U and ^{232}Th . In order to measure radioactivity at the aforementioned required level, we developed the first ultra-low background (BG) high-purity germanium (HPGe) detector in 2016, hereafter referred to as Ge01. This detector has been used to screen materials with high sensitivity [2, 5–8]. Then in 2020, we developed a new ultra-low BG HPGe detector with more careful treatment of the shielding material, to improve the sensitivity for increasing the capacity of material screenings for the second Gd-loading to Super-Kamiokande for 0.03% Gd concentration [K. Abe *et al.*, manuscript in preparation] and for future projects conducted at Kamioka.

This paper describes the performance of the newly installed HPGe detector, including its analysis procedure for measuring radioactivity. Sect. 2 provides details of the detector configuration, data acquisition system, and calibration results. Sect. 3 describes the data analysis, the time variation of the BG spectra, the comparison of the BG count rate with Ge01, and the sample measurement procedure. A summary is presented in Sect. 4.

2 Germanium Detector

2.1 Detector configuration

The new HPGe detector, hereafter referred to as Ge02, has been manufactured by Mirion Technologies France [9] with an ultra-low BG specification. Ge02 is a p-type coaxial detector with a crystal mass of 1.7 kg and a relative efficiency of $80\%^1$, the same specification as Ge01. The detectors are installed at the Kamioka Observatory in the Kamioka Mine under Mt. Ikenoyama. The average rock overburden is 2700 m water equivalent, which reduces the cosmic ray muon rate by 5 orders of magnitude. Fig. 1 illustrates the schematic view

¹ Efficiency is defined relative to a 3-inch diameter, 3-inch long NaI(Tl) crystal, for 1333 keV photopeak from a ^{60}Co source positioned 25 cm away from the detector.

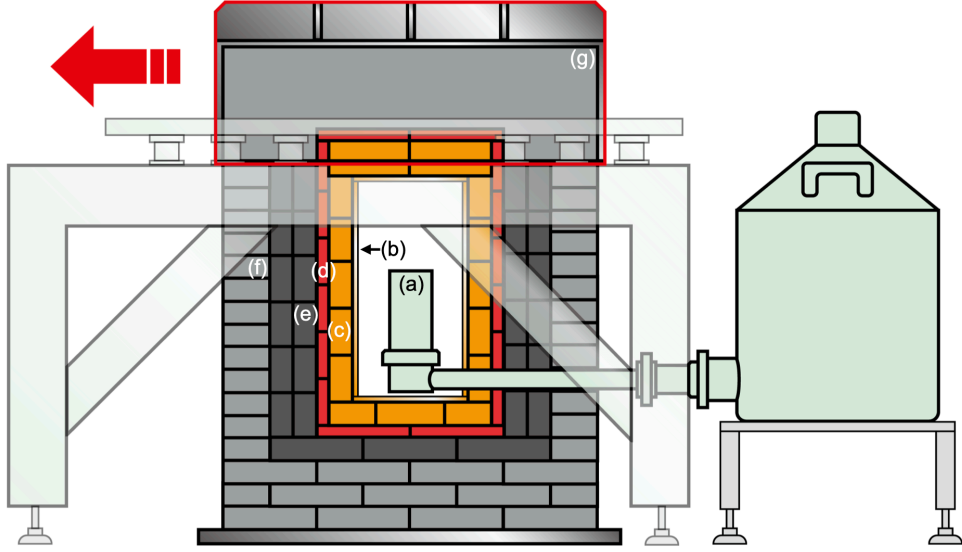


Fig. 1: Schematic view of the new HPGe detector. The HPGe detector with its cold finger and dewar (a), 6N grade copper (b), OFHC copper (c), lead layers with ^{210}Pb activities of $5\pm 3 \text{ Bq kg}^{-1}$ (d), $35\pm 4 \text{ Bq kg}^{-1}$ (e), $\mathcal{O}(100) \text{ Bq kg}^{-1}$ (f), and $\mathcal{O}(500) \text{ Bq kg}^{-1}$ (g, only for the top part) can be seen. The top part circled with the red line can be floated and moved.

of Ge02. The sample chamber has dimensions of $23\times 23\times 48 \text{ cm}^3$, with the HPGe detector positioned centrally within it. The Ge crystal is housed in a cylindrical endcap made of ultra-low BG aluminum. The spacious sample chamber allows the measurement of large sample quantities, such as 13×3 -inch photomultiplier tubes [7] and 10 kg of $\text{Gd}_2(\text{SO}_4)_3\cdot 8\text{H}_2\text{O}$ [2]. To mitigate the BG caused by radon (Rn) gas emanating from the shielding materials mentioned below, the sample chamber is continuously purged with Rn -free air at a rate of 5 standard liters per minute in which the concentration of ^{222}Rn is $< 1 \text{ mBq/m}^3$ [10]. The chamber is enveloped by 1 cm thick, 6N grade copper ($> 99.9999\%$ purity) supplied by Mitsubishi Materials Corporation [11]. Surrounding the 6N grade copper is a 5 cm layer of oxygen-free-high-conductivity (OFHC) copper that has been stored at the Kamioka mine for over a decade. These layers of copper act as a shield against bremsstrahlung radiation generated by the beta-rays of ^{210}Bi decay in the lead layers mentioned below. The OFHC copper is surrounded by a 2.5 cm lead layer with a ^{210}Pb activity of $5\pm 3 \text{ Bq kg}^{-1}$. Then there is a 5 cm lead layer for the bottom (10 cm for the side) with a ^{210}Pb activity of $35\pm 4 \text{ Bq kg}^{-1}$, purchased from SEIKO EG&G Co Ltd. [12]. Outside of these low ^{210}Pb lead layers are covered by lead with a ^{210}Pb activity of $\mathcal{O}(100) \text{ Bq kg}^{-1}$.

The upper part of the 5 cm OFHC copper layer and the lead layers can be floated and moved laterally using a frame guide. The innermost 2.5 cm of the lead layer in the top

section has a ^{210}Pb activity of $5\pm 3\text{ Bq kg}^{-1}$ and the remaining 17.5 cm lead layer has that of $\mathcal{O}(500)\text{ Bq kg}^{-1}$. In total, the lead layers have a combined thickness of 22.5 cm (20 cm for the top part) to shield against environmental gamma-rays. Ge01 and Ge02 have the same thickness of the Cu layer and the combined lead layers. The difference in the shield configuration between Ge01 and Ge02 is that Ge01 has a ^{210}Pb activity of $\mathcal{O}(100)\text{ Bq kg}^{-1}$ lead for the layer marked as (e, that of $35\pm 4\text{ Bq kg}^{-1}$) and [g, that of $\mathcal{O}(500\text{ Bq kg}^{-1})$] in Fig. 1. The newly purchased 6N grade copper and lead bricks with a ^{210}Pb activity of $5\pm 3\text{ Bq kg}^{-1}$ underwent a cleaning process involving immersion in 4% dilute nitric acid for 20 minutes, followed by rinsing with ultra-pure water for an additional 20 minutes to remove surface contamination. These materials were then wiped with a clean cloth and dried in a chamber supplied with nitrogen gas flowing at a rate of 5 standard liters per minute for a day. Other copper and lead bricks were cleaned with ethanol prior to installation. As for the cleaning process for 6N copper and lead bricks with a ^{210}Pb activity of $5\pm 3\text{ Bq kg}^{-1}$ used in Ge01 shield layers, they were only cleaned with ethanol using an ultrasonic cleaning machine. Typically, normal samples are placed on a 5 mm thick acrylic stage. The distance between the top of the acrylic stage and the end cap of the Ge detector is 9 mm. However, for measuring a large amount of sample, such as the 10 kg $\text{Gd}_2(\text{SO}_4)_3\cdot 8\text{H}_2\text{O}$ mentioned in Sect. 3, the acrylic stage can be removed, allowing the sample piece to be placed next to the Ge detector.

2.2 Data acquisition system

The signal from the Ge02 detector preamplifier was fed into a Canberra Model 2026 main amplifier. The signal from both the preamplifier and the main amplifier was recorded by a CAEN DT5724B waveform digitizer with a sampling rate of 100 MHz. The coarse and fine gain settings of the main amplifier were adjusted to avoid saturation of the Analog-to-Digital Converter (ADC) of the waveform digitizer by the ^{208}Tl 2614 keV photopeak. Fig. 2 shows the typical waveform of the ^{137}Cs 662 keV photopeak event. The threshold of the main amplifier waveform is 30 ADC counts above the baseline, corresponding to an energy threshold of about 10 keV. For energy estimation, the maximum amplitude of the pulse from the main amplifier and a baseline calculated from the first 2 μs of the waveform were used. Pulse information such as the baseline fluctuation and the channel at the maximum amplitude facilitates the identification and rejection of unphysical electric noise events and pile-up events.

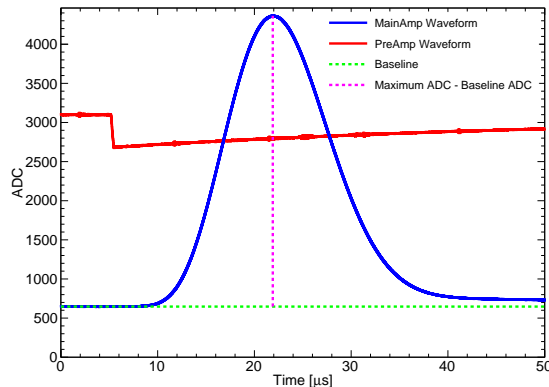


Fig. 2: Typical preamplifier and main amplifier waveforms for a ^{137}Cs 662 keV photopeak event. The horizontal dashed line represents the baseline level calculated from the first $2\ \mu\text{s}$ of the waveform. The vertical dashed line corresponds to the amplitude of the maximum peak observed in the output signal of the main amplifier. This value is obtained by subtracting the baseline ADC from the peak height and is used to estimate the energy associated with the detected gamma-ray event.

2.3 Calibration measurement and efficiency determination

Detector calibrations have been performed regularly using radioactive sources of ^{60}Co , ^{133}Ba , and ^{137}Cs . Fig. 3 shows the linearity of the energy response and the energy resolution as a function of the energy. Energy is calibrated within 0.06% uncertainty. The full width at half maximum (FWHM) of the 1333 keV photopeak of ^{60}Co was measured to be 1.82 keV. In the comparison between the energy spectra of the experimental data and the Monte Carlo (MC) simulations, the energy resolution function shown in Fig. 3 (right) is used.

The MC simulations based on Geant4 [13] are performed to compute the detection efficiencies for different gamma-lines used to assess radioactivities, as described in Sect. 3.2. These simulations take into account the detailed geometry of the detector, including the shielding layers. Fig. 4 shows a comparison between the spectra obtained from the ^{60}Co , ^{133}Ba , and ^{137}Cs calibrations and those obtained from the simulations which trace the full decay chain of the isotopes using G4RadioactiveDecay. Except for an unknown continuous component excess of data below 60 keV, the simulation reproduces the calibration data well. The peak count rates observed in the calibration data, with the source placed at different positions, agree within 10% with those obtained from the MC simulation. Following the approach outlined in Refs. [7, 14], since the systematic uncertainties associated with

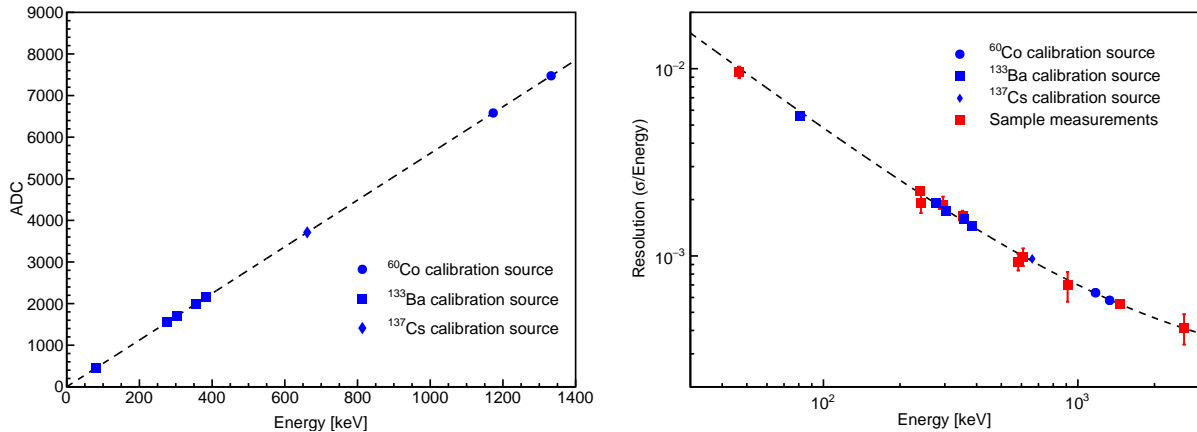


Fig. 3: (Left) Linearity of the energy response and (right) energy resolution, defined as the σ divided by the energy, obtained from calibration sources and sample measurements. The dashed curve represents a fitted result of $\sigma^2(E) = E^2[(4.95 \pm 1.07) \times 10^{-8}] + E[(2.31 \pm 0.24) \times 10^{-4}] + [(2.09 \pm 0.10) \times 10^{-1}]$ using calibration sources.

the detection efficiencies derived from the simulation are common to all measurements, the results presented in Sect. 3.2 are given only with their respective statistical uncertainties.

3 Data analysis methods

3.1 Background spectra

Data acquisition with the shielding described in Sect. 2.1 started in December 2021. During the sample measurements described in Sect. 3.2, three long-term BG data acquisitions were performed. Fig. 5 shows the time variation of the BG spectra. The continuous component and the distinct peaks due to cosmogenic activation in germanium and copper, as mentioned in Ref. [15], such as ^{57}Co (122 keV, $T_{1/2} = 271.74$ d) and ^{58}Co (811 keV, $T_{1/2} = 70.86$ d), show a decreasing trend with time. The peaks attributed to ^{210}Pb and ^{137}Cs , which were observed in the energy spectra of Ge01 (Fig. 6 in Ref. [2]), also show a significant decrease from Ge01.

Table 1 shows the BG count rate for the integral in the energy range from 40 to 2700 keV, as well as for several gamma-lines. After the decrease of radioactivity due to cosmogenic activation, the integral count rate in the energy range from 40 keV to 2700 keV of Ge02 becomes 25% lower than that of Ge01. Table 2 summarizes the crystal mass, energy resolution and BG count rate in comparison with other ultra-low BG HPGe detectors used for material

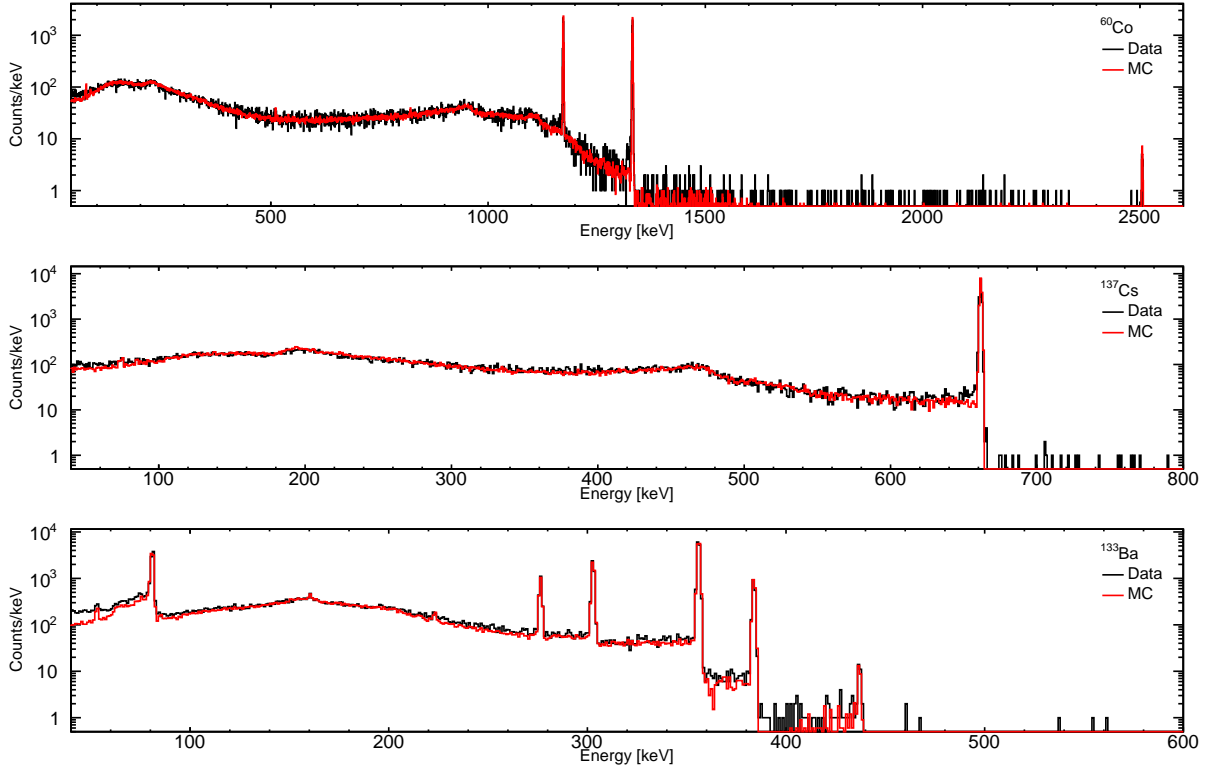


Fig. 4: Comparison of the energy spectrum from ^{60}Co (top), ^{137}Cs (middle), and ^{133}Ba (bottom) calibration data with that of a Monte Carlo simulation. In the simulation, the energy spectrum is normalized by the measurement time and the activity of the source, and the energy deposition in the HPGe detector is smeared with the energy resolution function described in Fig. 3. The differences of the count rate $(\text{MC} - \text{Data})/\text{Data}$ in the $\pm 3\sigma$ region, subtracting the continuous count rate derived from the sideband region, are $-16.5 \pm 6.9\%$ (^{133}Ba , 53 keV), $7.6 \pm 1.1\%$ (^{133}Ba , 81 keV), $1.8 \pm 2.3\%$ (^{133}Ba , 277 keV), $5.1 \pm 1.4\%$ (^{133}Ba , 303 keV), $4.5 \pm 0.8\%$ (^{133}Ba , 356 keV), $8.3 \pm 2.1\%$ (^{133}Ba , 384 keV), $11.4 \pm 0.9\%$ (^{137}Cs , 662 keV), $9.5 \pm 1.3\%$ (^{60}Co , 1173 keV), $9.7 \pm 1.3\%$ (^{60}Co , 1333 keV), respectively. Here error values correspond to the statistical uncertainties.

screening at the other experimental site. The BG level of Ge02 is comparable to that of the HPGe detectors used for material screening at the most advanced experiments.

3.2 Sample measurements

Samples are flushed with Rn-free air, evacuated, and sealed in ethylene-vinyl alcohol (EVOH) bags. EVOH bags retain Rn emanated from samples. Fig. 6 shows photographs of a 440 g PEN pellet sample and a 10 kg of $\text{Gd}_2(\text{SO}_4)_3 \cdot 8\text{H}_2\text{O}$ sample.

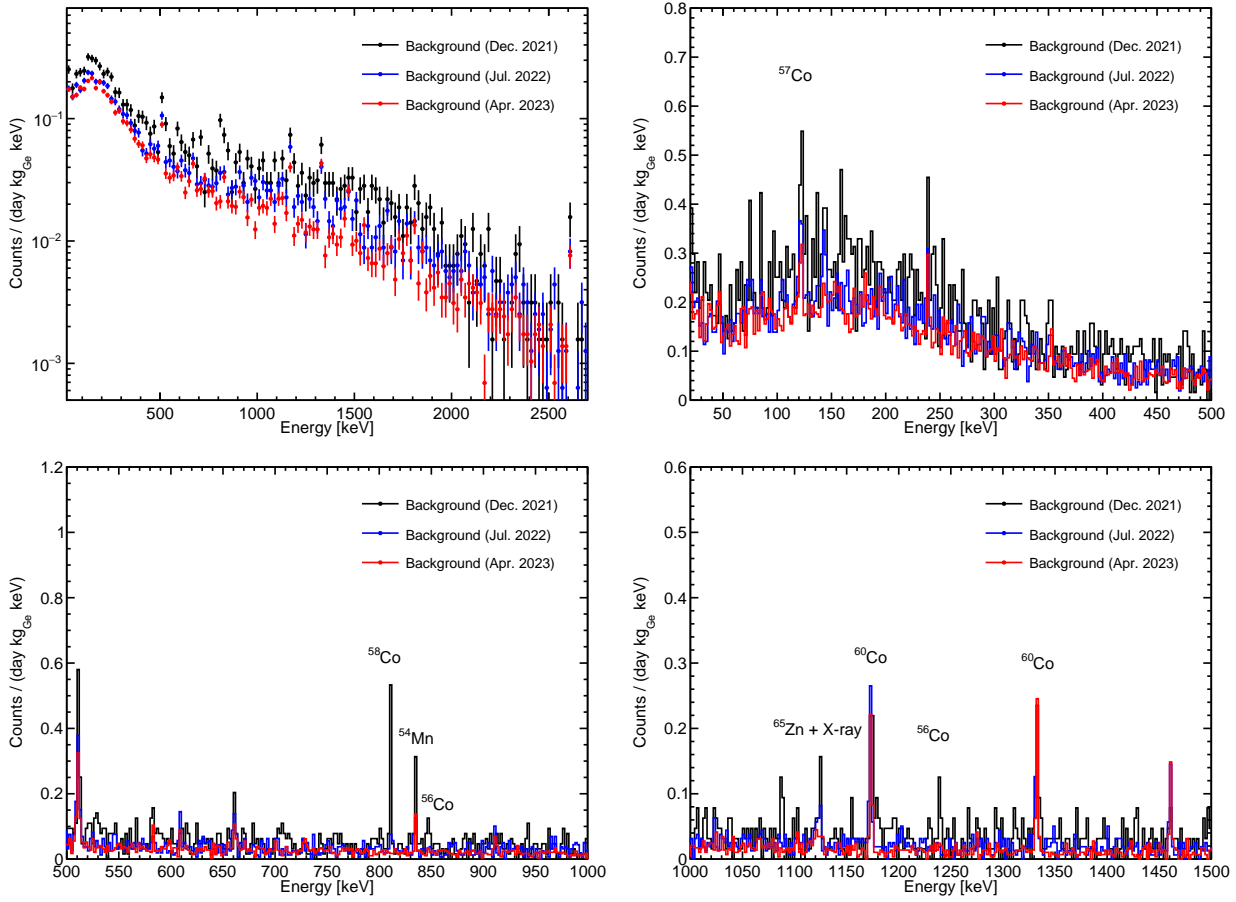


Fig. 5: The energy spectrum of the background data taken on December 2021, July 2022, and April 2023 for the energy ranges of $[20,2700]$ keV (top left, 20 keV bin, with statistical error bar), $[20, 500]$ keV (top right), $[500, 1000]$ keV (bottom left), and $[1000,1500]$ keV (bottom right). The bin width for the linear-scale figures is 2 keV. Clear peaks induced by cosmogenic activation in germanium and copper are listed in the linear-scale figures.

Data collected within the first 12 hours from sample deployment were not used in the analysis to mitigate the effects of Rn which was contaminated into the chamber during the sample deployment. A noisy period associated with the supply of liquid nitrogen was also excluded from the analysis. Figs. 7 and 8 show the energy spectra of the sample and the BG measurements.

The determination of the radioactivity of the sample is based on the net signal count S_{net} , which is defined as:

$$S_{net} = S_{peak} - S_{comp} - (B_{peak} - B_{comp}) \cdot T_s/T_b, \quad (1)$$

Table 1: The time variation of the background count rates for the integral in the 40–2700 keV region and integral count rates in the $\pm 3\sigma$ region for several gamma-lines. For the Ge01 detector, the count rates are calculated from the background data used in Ref. [2].

Detector	Ge01		Ge02	
Date	Dec. 2019	Dec. 2021	Jul. 2022	Apr. 2023
Measurement time (d)	23.0	19.0	47.2	86.2
Count rate ($\text{kg}_{\text{Ge}}^{-1} \text{day}^{-1}$)				
Integral 40 – 2700 keV	112.6	140.2	100.0	84.3
^{208}Tl , 2614 keV	0.08 ± 0.04	0.25 ± 0.09	0.16 ± 0.05	0.13 ± 0.03
^{214}Bi , 609 keV	0.39 ± 0.10	0.25 ± 0.09	0.38 ± 0.07	0.23 ± 0.04
^{60}Co , 1333 keV	0.41 ± 0.10	0.66 ± 0.14	0.48 ± 0.08	0.68 ± 0.07
^{40}K , 1461 keV	0.44 ± 0.11	0.31 ± 0.10	0.44 ± 0.07	0.42 ± 0.05
^{137}Cs , 662 keV	1.29 ± 0.18	0.53 ± 0.13	0.38 ± 0.07	0.32 ± 0.05
^{210}Pb , 46.5 keV	3.24 ± 0.29	0.69 ± 0.14	0.64 ± 0.09	0.59 ± 0.06

Table 2: Comparison of crystal mass, relative efficiency, energy resolution and background rate with other HPGe detectors used for material screening at the other underground experimental site. The HPGe detectors described in Refs. [2, 16] are listed.

Site	Detector	Crystal mass [kg]	Relative efficiency [%]	FWHM at 1333 keV [keV]	BG rate 60 – 2700 keV [$\text{kg}_{\text{Ge}}^{-1} \text{day}^{-1}$]
Kamioka	Ge02 (This work)	1.68	80	1.82	81.3 ± 0.7
	Ge01 [2]	1.68	80	2.39	104.5
LNGS	Gator [16]	2.2	100.5	1.98	89.0 ± 0.7
	GeMPI [16]	2.2	98.7	2.20	24 ± 1
BUGS	Belmont [2]	3.2	160	1.92	90.0
	Merrybent [2]	2.0	100	1.87	145.0
LSC	GeOroel [2]	2.31	109	2.22	128.7
	Asterix [2]	2.13	95.1	1.92	171.3
	GeAnayet [2]	2.26	109	1.99	461.2
BHUC	Maeve [17]	2.0	85	3.19	956.1
LVdA	GeMSE [16, 18]	2.0	107.7	1.96	88 ± 1

Here, S_{peak} represents the counts in the photopeak region. The photopeak region is defined as the ± 4 keV region from the peak, that is sufficiently larger than the energy scale uncertainty and $\pm 3\sigma$ of the energy resolution. S_{comp} corresponds to the Compton BG counts and is estimated from the ± 4 keV regions adjacent to the photopeak region. B_{peak} and B_{comp}



Fig. 6: Pictures of a 440 g PEN pellet sample on the acrylic sample stage(left) and Ge02 detector with 10 kg of $Gd_2(SO_4)_3 \cdot 8H_2O$ sample (right).

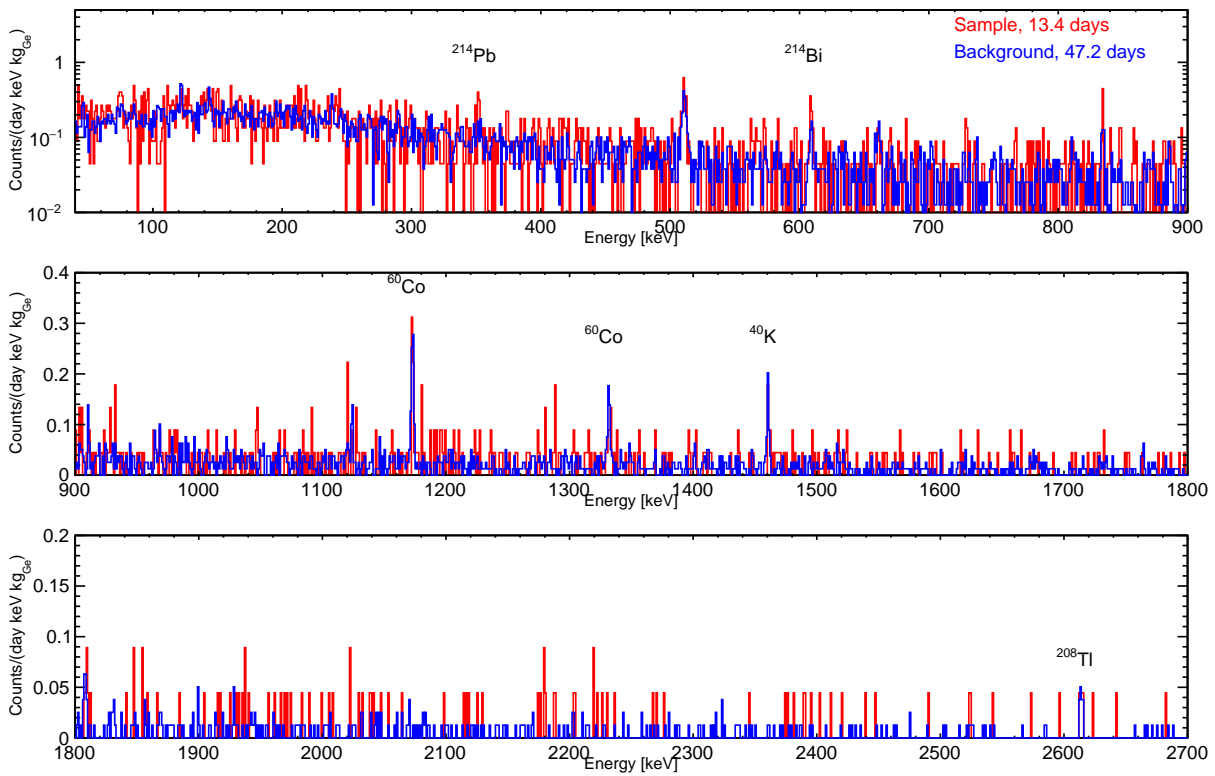


Fig. 7: The energy spectra for the PEN pellet sample measurement and the background.

denote the counts in the photopeak and Compton regions of the BG data, respectively. T_s and T_b are the measurement times for the sample and the BG, respectively.

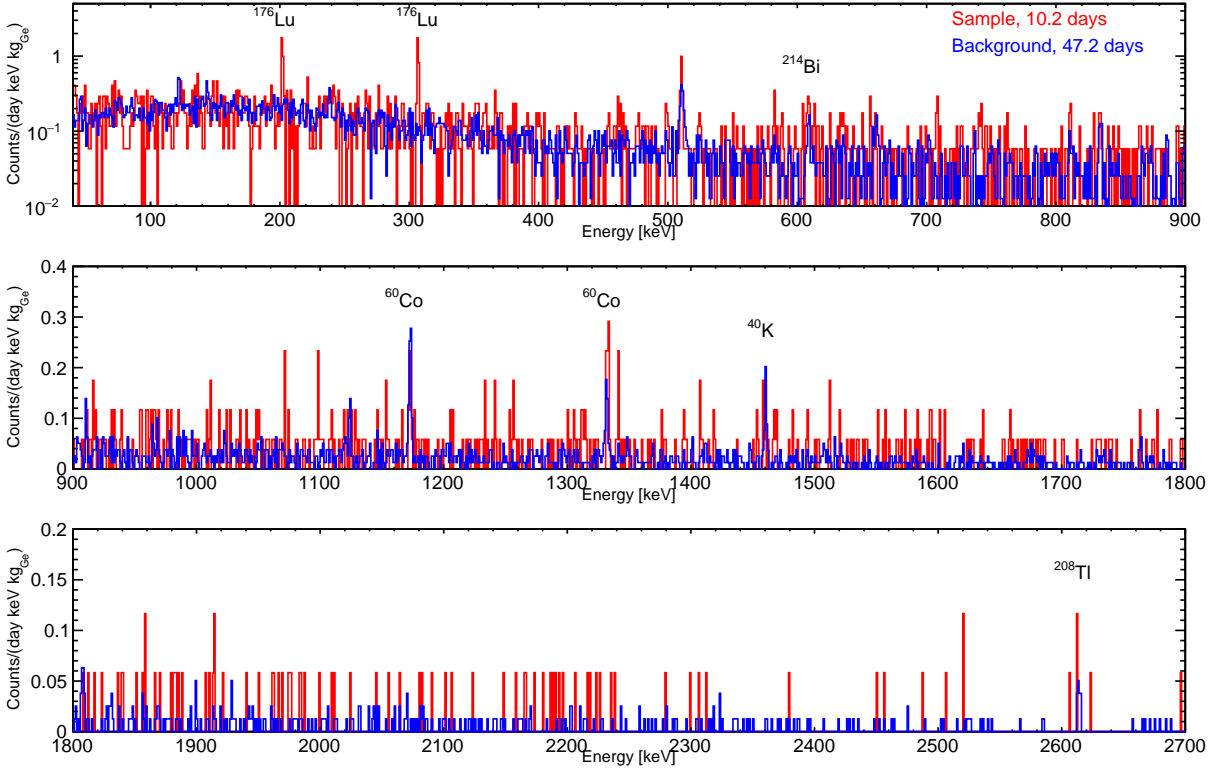


Fig. 8: The energy spectra for a typical 10 kg of $\text{Gd}_2(\text{SO}_4)_3 \cdot 8\text{H}_2\text{O}$ sample measurement and the background.

The specific activity A [Bq kg^{-1}] for a given gamma-line is determined using the equation:

$$A [\text{Bq kg}^{-1}] = \frac{S_{net}}{I_\gamma \cdot \epsilon \cdot m \cdot T_s}. \quad (2)$$

In this equation, I_γ represents the branching ratio of the gamma-ray, ϵ is the photopeak detection efficiency and m is the mass of the sample in kilograms. The term ϵ is evaluated by the MC simulation using regular-shaped geometry closest to that of the sample. The density and composition of the sample are also taken into account by the MC to consider self-absorption in the samples. The simulated monochromatic gamma-rays are generated uniformly and isotropically within the sample volume. If several prominent gamma-lines originate from a specific radioisotope (RI), the radioactivity is determined using the weighted average of the evaluations for each gamma-line. For example, gamma-lines from ^{214}Pb (295 keV) and ^{214}Bi (609, 1120, and 1764 keV) are used to assess the radioactivity of ^{226}Ra . The effect of the coincidence sum of multiple gamma-rays in the decay cascade was simulated for these samples and found to be negligible compared to the statistical error. Following Refs. [7, 14], if

the central value does not exceed twice the statistical error or is negative, the result is considered to be consistent with zero. In such cases, an upper limit at the 90% confidence level (C.L.) is calculated as $\max\{0, \text{the central value}\} + 1.28 \times \text{the statistical error}$. Table 3 shows the measured RIs for the PEN pellet and $\text{Gd}_2(\text{SO}_4)_3 \cdot 8\text{H}_2\text{O}$ samples. With the exception of ^{176}Lu in the $\text{Gd}_2(\text{SO}_4)_3 \cdot 8\text{H}_2\text{O}$ sample, no significant RIs were observed. Similar to Ge01, Ge02 demonstrates sensitivity to less than 0.5 mBq kg^{-1} of ^{226}Ra in the $\text{Gd}_2(\text{SO}_4)_3 \cdot 8\text{H}_2\text{O}$ sample at a 90% C.L. with about 10 days of measurement.

Table 3: Summary of the measurement results [mBq kg^{-1}] for PEN pellet and $\text{Gd}_2(\text{SO}_4)_3 \cdot 8\text{H}_2\text{O}$ sample. Upper limits correspond to the 90% confidence level.

Sample	PEN Pellet	$\text{Gd}_2(\text{SO}_4)_3 \cdot 8\text{H}_2\text{O}$
Measurement time [d]	13.4	10.2
Early part of ^{238}U chain		
^{234}Th 63, 93 keV	< 17.4	< 6.2
$^{234\text{m}}\text{Pa}$ 1001 keV		
middle part of ^{238}U chain		
^{214}Pb 295 keV	< 2.60	< 0.43
^{214}Bi 609, 1120, 1764 keV		
late part of ^{238}U chain		
^{210}Pb 46.5 keV	< 137	< 91
Early part of ^{232}Th chain		
^{228}Ac 338, 911, 969 keV	< 2.10	< 0.25
late part of ^{232}Th chain		
^{212}Bi 727 keV	< 1.96	< 0.16
^{208}Tl 583, 861, 2614 keV		
Early part of ^{235}U chain		
^{235}U 144, 163, 205 keV	< 5.56	< 1.79
late part of ^{235}U chain		
^{223}Ra 154, 269 keV	< 3.47	< 0.66
^{219}Rn 271, 402 keV		
^{211}Pb 405, 427, 832 keV		
^{40}K 1461 keV	< 7.63	< 0.86
^{60}Co 1173, 1333 keV	< 0.66	< 0.07
^{176}Lu 202, 307 keV	< 0.52	0.46 ± 0.09

Almost all $\text{Gd}_2(\text{SO}_4)_3 \cdot 8\text{H}_2\text{O}$ lots used in the second Gd-loading to Super-Kamiokande were screened with the Ge01 and Ge02 detectors. Further details on the screening of $\text{Gd}_2(\text{SO}_4)_3 \cdot 8\text{H}_2\text{O}$ will be found in K. Abe *et al.* [manuscript in preparation].

4 Conclusion

We have successfully deployed a new low-background HPGe detector at the Kamioka Observatory. The integral background count rate in the energy range from 40 keV to 2700 keV is about 25% lower than that of Ge01 and comparable to that of the HPGe detectors used for material screening at the most advanced experiments. The HPGe detector demonstrates a sensitivity of less than 0.5 mBq kg^{-1} of ^{226}Ra in a 10 kg $\text{Gd}_2(\text{SO}_4)_3 \cdot 8\text{H}_2\text{O}$ sample at a 90% C.L. with an approximate measurement time of 10 days. This detector is currently playing essential roles for material screenings for the SK-Gd, KamLAND-Zen, and other research and development experiments.

Acknowledgment

We thank Mirion Technologies staff for fruitful discussions and the development of an ultra-low BG HPGe detector. We would like to thank Toyobo Co., Ltd. and Nippon Yttrium Co., Ltd. for providing the samples. We thank the technical staffs of the RCNS and ICRR for their assistance with the detector installation work. This work was supported by the Japanese Ministry of Education, Culture, Sports, Science and Technology, Grant-in-Aid for Scientific Research, JSPS KAKENHI Grant No. 19H05807, 19H05808, 21H01105, the joint research program of the Institute for Cosmic Ray Research (ICRR), the University of Tokyo.

References

- [1] J. F. Beacom and M. R. Vagins, *Phys. Rev. Lett.*, **93**, 171101 (2004).
- [2] K. Hosokawa et al., *Progress of Theoretical and Experimental Physics*, **2023**(1), 013H01 (12 2022).
- [3] S. Abe et al. (KamLAND-Zen Collaboration), *Phys. Rev. Lett.*, **130**, 051801 (Jan 2023).
- [4] S Obara, Y Gando, and K Ishidoshiro, *Progress of Theoretical and Experimental Physics*, **2019**(7), 073H01 (07 2019).
- [5] S. Ito et al., *Progress of Theoretical and Experimental Physics*, **2018**(9), 091H01 (09 2018).
- [6] S. Ito et al., *Progress of Theoretical and Experimental Physics*, **2020**(9), 093H02 (09 2020).
- [7] K. Abe et al. (XMASS collaboration), *Journal of Instrumentation*, **15**(09), P09027–P09027 (sep 2020).
- [8] Y. Nakano et al., *Progress of Theoretical and Experimental Physics*, **2020**(11), 113H01 (11 2020).
- [9] Mirion Technologies (Canberra) France SAS, <https://www.mirion.com> (data last accessed 2023-08-08).
- [10] Y. Nakano et al., *Nuclear Instruments and Methods in Physics Research Section A: Accelerators, Spectrometers, Detectors and Associated Equipment*, **867**, 108–114 (2017).
- [11] Mitsubishi Materials, <https://www.mitsubishi-copper.com/en/> (data last accessed 2023-08-08).
- [12] Seiko EG&G Co. Ltd., <https://www.sii.co.jp/en/> (data last accessed 2023-08-08).
- [13] S. Agostinelli et al. (Geant4 collaboration), *Nuclear Instruments and Methods in Physics Research Section A: Accelerators, Spectrometers, Detectors and Associated Equipment*, **506**(3), 250–303 (2003).
- [14] K. Abe et al. (XMASS Collaboration), *Nuclear Instruments and Methods in Physics Research Section A: Accelerators, Spectrometers, Detectors and Associated Equipment*, **922**, 171–176 (2019).

- [15] S. Cebrián et al., *Astroparticle Physics*, **33**(5), 316–329 (2010).
- [16] Gabriela R. Araujo et al., *Journal of Instrumentation*, **17**(08), P08010 (Aug 2022).
- [17] D. S. Akerib et al. (LZ Collaboration), *The European Physical Journal C*, **80**(11), 1044 (2020).
- [18] D. Ramírez García et al., *Journal of Instrumentation*, **17**(04), P04005 (Apr 2022).